Supporting Information

Superelastic hydrogel electrolyte incorporating helical protein molecules as zinc ion transport pathways to enhance cycling stability of zinc metal batteries

Xiaoyun Xu[a], *Songmei Li*[a], *Shubin Yang*[a], *Bin Li*[a]*
a School of Materials Science & Engineering, Beihang University, Beijing, 100191, China
*E-mail: li_bin@buaa.edu.cn

Experiment Section

Materials

All chemicals were of analytical grade and used directly after purchase without further purification. Propanone, ethyl alcohol, urea, sodium dodecyl sulfate (SDS), sodium sulfide (Na_2S), polyvinyl alcohol, glycerol and zinc trifluoromethanesulfonate were purchased from aladdin.

Preparation of α-HP

α-HP was prepared by a reduction method.[1] Firstly, wool fibers were soaked in acetone for 4 h and subsequently washed three times with ethanol to remove oils and impurities. The washed wool fibers (5 g) were immersed in a 50 mL aqueous solution containing 8M urea (24.024 g), 0.1M SDS (1.442 g), and 0.1M Na_2S (0.390 g), and stirred at 60 °C for 8 h. After that, the yellow crude keratin solution was obtained by filtration, and then dialyzed with dialysis bags (molecular weight cut-off of 3,500 D) in deionized water for 3 d to remove the protein denaturants and reducing agents. During the dialysis process, the deionized water was changed every 3 h, and the volume ratio of deionized water to dialysate was maintained at about 100:1. Finally, the above keratin solution was concentrated to 20 mL and freeze-dried to obtain white α-HP powder.

Preparation of α-HP/PVA and PVA hydrogel electrolyte

Firstly, 0.88 g P-VA (polyvinyl alcohol) and 0.12 g glycerol were added to 5 mL of deionized water and stirred at 90 °C for 5 h to obtain a homogeneous PVA solution. And 0.88 g α-HP and 3.63 g $Zn(OTf)_2$ were added to 5 mL of deionized water and stirred at room temperature for 2 h to obtain a homogeneous α-HP solution. Then, the PVA solution and α-HP solution were mixed and stirred at room temperature for 1 h to obtain the α-HP/PVA solution. Finally, the α-HP/PVA solution was poured into a mold and kept at low temperature overnight (2~5°C) to obtain the α-HP/PVA hydrogel electrolyte.

The preparation process of the PVA hydrogel electrolyte was consistent with that of α-HP/PVA, except that there was no addition of 0.88 g of α-HP.

Preparation of NaV_3O_8-1.5H_2O (NVO) cathode materials

Firstly, 1.753 g of NaCl and 1.000 g of V_2O_5 were added to 15 mL of deionized water and then stirred vigorously for 96 h in an airtight environment at 30°C. After that, the brick-red mixture was centrifuged at 5000 rpm for 5 mins for three times. Finally, the brick-red NaV_3O_8-1.5H_2O active material was obtained by freeze-drying.[2]

70 wt.% of the active material (NVO), 20 wt.% of the conductive carbon (Super P) and 10 wt.% of the binder polyvinylidene fluoride (PVDF) were mixed in N-Methylpyrrolidone (NMP) and ground for 30 min. Then, the obtained cathode slurry was coated onto the carbon paper by a simple blade coating method. Finally, the NVO cathodes were obtained by drying under vacuum at 70 °C for 12 h with an active material of about 2~5 mg cm^{-2}.

Material Characterizations

Atomic force microscope (AFM Dimension IconXR) and scanning electron microscope (SEM JSM7500 or JSM6010) was performed to observe the morphology and microstructure of electrode surface and gel matrix. X-ray diffraction (XRD D/MAX2200pc) with Cu-Kα1 radiation (λ=1.5406Å) was performed to identify the components and phase information of electrode surface. Raman spectra and Fourier Transform infrared spectroscopy (FTIR Thermo Scientific Nicolet iS50) were performed to study chemical structure and property of the electrolyte. Elements valence information of anode surface and gel electrolyte were obtained by x-ray photoelectron

spectroscopy (XPS Thermo Scientific K-Alpha). 3D microscope was used to study the morphology of the electrode surface after cycling. The cupping machine (WDW-5) was used to test the stress-strain curve of the gel electrolyte. Transmission electron microscopy (TEM) was used to characterize the crystal structure information of SEIs, and TEM samples were prepared by focused ion beam (FIB).

Scanning Kelvin Probe (SKP) was used to characterise the evolution of the passivation layer in micro-regions on the electrode surface. SKP, a micro electrochemical technique, is used to characterize the electrochemical information on the surface of the specimens[3]. SKP potential maps and the corresponding Gauss fitting curves for SKP potential are exhibited in **Figure 3g** and **Figure S21**. The Gauss fitting formula is shown in following:

$$y = y_0 + \frac{A}{\sigma\sqrt{\frac{\Pi}{2}}} e^{-2\left(\frac{x-\mu}{\sigma}\right)^2}$$

where A is a constant, y_0 is the offset of the vertical axis, μ is the concentrated position of SKP potential distribution, σ is the degree of concentration of SKP potential distribution. The smaller the value of σ, the more concentrated the potential distribution is on the value of μ.

Electrochemical measurements

For the standardization of the measurements, all electrodes with a diameter of 10 mm were used in the assembly of the button cell, and 2M $Zn(OTf)_2$ or α-HP/PVA electrolyte was used as the electrolyte, respectively. The reference group used 19 mm diameter glass fiber as the separator. All cyclic voltammetry (CV) and electrochemical impedance spectroscopy (EIS) tests were performed using a two-electrode system unless otherwise noted.

The Zn||Zn symmetric cell and the Zn||Cu half cell were assembled using 2032 coin cells with different electrolytes. In the symmetric cell test, the cells were cycled at 1 mA cm^{-2} and 0.1 mA cm^{-2} with a capacity of 1 mAh cm^{-2}. To eliminate the effect of uncertainties associated with the substrate (surface roughness and handling conditions) on subsequent cycling, coulombic efficiencies of the different electrolytes were measured in "mixed mode". All cell tests were performed on a CT2001A cell test

instrument (LAND Electronic Co, BT2013A, China). Cyclic voltammetry (CV) analysis, linear scanning voltammetry (LSV) analysis, Tafel curve and electrochemical impedance spectroscopy (EIS) analysis were performed on an electrochemical workstation (CHI660E). The LSV test was performed with the three-electrode configuration (bare zinc as working electrode, platinum electrode as counter electrode, saturated calomel electrode as reference electrode), and the scan rate is 5 mV s^{-1} and scan range is 0 ~ -2 V.

Full cells measurements

The full cell was assembled into a button cell (2032 button cell) with NVO cathode, bare zinc anode and glass fibers separator. The electrolyte was 2M $Zn(OTf)_2$ or α-HP/PVA. The full cell was cycled between 0.3 and 1.25 V at 1 A g^{-1} and 10 A g^{-1} . The rate performance and full-cell performance were performed on a CT2001A cell test instrument (LAND Electronic Co, BT2013A, China). The full cell CV analysis was performed on an electrochemical workstation (CHI660E) with a scan rate of 1 mV s^{-1} and a scan range of 0.3 to 1.25 V.

The pouch cells were assembled by a thermal encapsulation process using an aluminum-plastic packaging film, and the electrodes and electrolytes were NVO cathode, bare zinc anode, and α-HP/PVA hydrogel electrolyte. Two sizes of pouch cells (4×5 cm and 5×10 cm) were assembled, and all pouch cells were constructed with a single layer. In the 4×5 cm size pouch cell, the loading of NVO was about 3 mg cm^{-2}. In the 5×10 cm size high loading pouch cell, the loading of NVO was about 10 mg cm^{-2}.

pH measurement

The preparation of α-HP/PVA hydrogel electrolytes requires low temperature treatment (2 ~ 5 °C), which is a α-HP/PVA solution before low temperature treatment. First, we compared the pH of the α-HP/PVA hydrogel electrolyte and the α-HP/PVA solution by precision pH test paper, and the result showed that the pH of the two states were close, which indicated that the low temperature treatment did not affect the electrolyte pH. Therefore, to make the pH testing more convenient, we directly tested the pH of the α-HP/PVA solution by pH meter.

Density Functional Theory (DFT) calculation

All DFT calculations were carried out by the Vienna Ab initio Simulation Package (VASP) program, and numerical simulations were performed using the projected augmented wave (PAW) method[4]. The generalized gradient approximation (GGA) of Perdew-Burke-Ernzerhof (PBE) was used. In the geometry optimization process, the plane-wave cutoff energy of the valence electrons was considered to be set to 350 eV, and a 3 × 3 × 1 Monkhorst-Pack k-mesh is used for the Brillouin zone. The zinc metal (002), (100) and (101) crystal planes were fixed for the calculations. In addition, the electrostatic potential (ESP) of H_2O, P-VA and α-HP was calculated using GaussView software package.

The adsorption energy (E_{adsorb}) between the different crystalline surfaces of Zn and the H_2O/PVA/α-HP molecules was calculated using DFT with the following formula：

$$E_{adsorb} = E_{Zn+H2O/P-VA/\alpha-HP} - (E_{Zn} + E_{H2O/P-VA/\alpha-HP})$$

where $E_{Zn+\ H2O/P\text{-}VA/\alpha\text{-}HP}$ is the total energy of Zn and H_2O/P-VA/α-HP, E_{Zn} is the energy of Zn, and $E_{H2O/P\text{-}VA/\alpha\text{-}HP}$ is the energy of H_2O, PVA or α-HP molecule.

Performance optimisation of hydrogel electrolyte

The physical cross-linking is used to prepare hydrogel electrolytes, and the effect of different polyvinyl alcohol contents on hydrogel formation is firstly explored. Through experimental comparison, 0.88 g P-VA (10 mL H_2O) is finally determined to be used for the preparation of hydrogel electrolytes. Then the hydrogel electrolyte with high ionic conductivity and good mechanical properties is obtained by regulating the content of α-HP and zinc salt. The effects of different α-HP contents on the physical properties and ionic conductivity of hydrogel electrolytes are explored (the zinc salt content is fixed at 3.63 g, about 1M) , with the increase of α-HP the physical structure of hydrogel electrolytes is more stable (**Figure S1a**), which is due to the fact that more α-HP with good mechanical properties participated in the construction of the hydrogel network. Within a certain range, the ionic conductivity of the hydrogel electrolyte increased with the increase of α-HP content, and the highest ionic conductivity (93.8 mS/cm) is achieved at α-HP content of 5.67 wt.% (about 0.88 g), which may be attributed to the α-HP providing a faster pathway for Zn^{2+} conduction (**Figure S2a**).

Then the effects of different Zn salt contents on the physical properties and ionic conductivity of the hydrogel electrolyte is also explored (α-HP content is fixed at 0.88 g). As shown in **Figure S1b**, the structure of the hydrogel electrolyte gradually softens until collapses with the increase of Zn salt content, which may be due to the fact that too high Zn salt content is unfavourable to the cross-linking between PVA and α-HP. Both too little and too much Zn salt are unable to obtain a high ionic conductivity (**Figure S2b**), which suggests that an appropriate Zn salt and a stable α-HP/PVA hydrogel skeleton are the preconditions for achieving rapid Zn^{2+} conduction.

In summary, a hydrogel electrolyte (α-HP/PVA) with high ionic conductivity (93.8 mS/cm) and good physical properties can be obtained by using 5.67 wt.% (0.88 g) PVA, 5.67 wt.% (0.88 g) α-HP and 23.4 wt.% (3.63 g) Zn salt. The specific compositional parameters of the hydrogel electrolytes are shown in **Table 2**. The intrinsic reasons for achieving high ionic conductivity would be discussed in the main text.

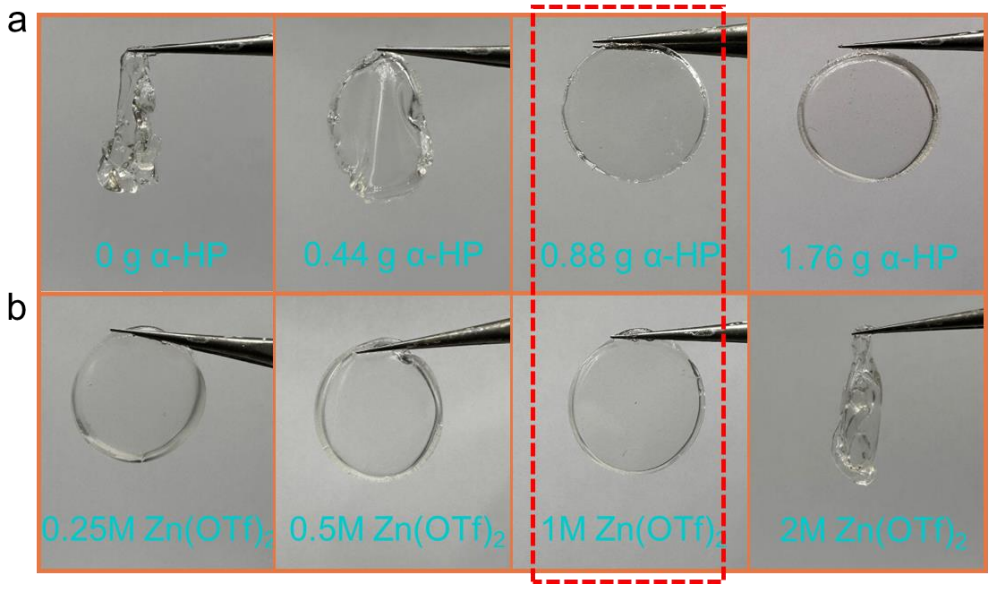

Figure S1. Comparison of optical photographs of hydrogel electrolytes with different α-HP (a) and Zn salt (b) contents.

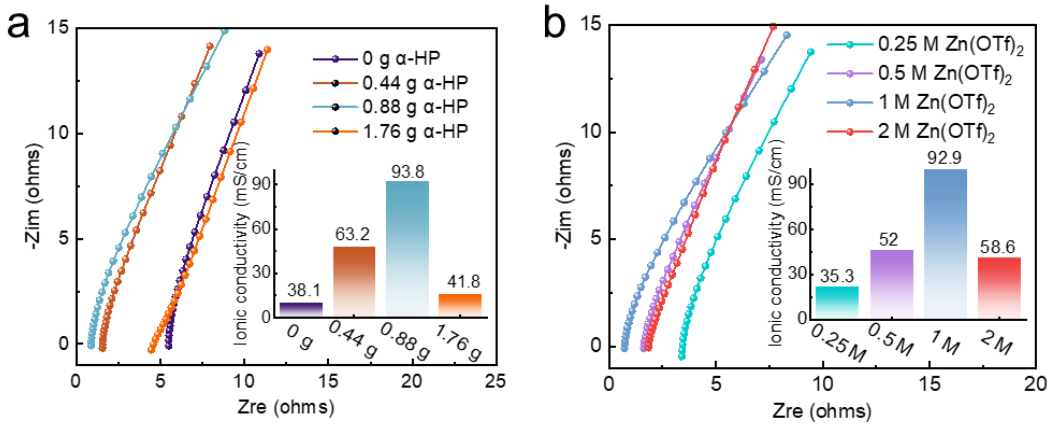

Figure S2. Ionic conductivity of hydrogel electrolytes with different α-HP (a) and Zn salt (b) contents.

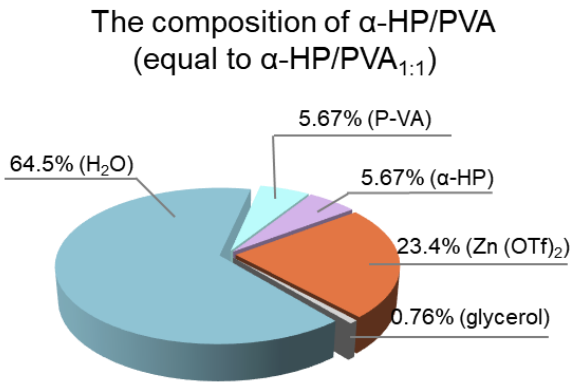

Figure S3. The composition of α-HP/PVA.

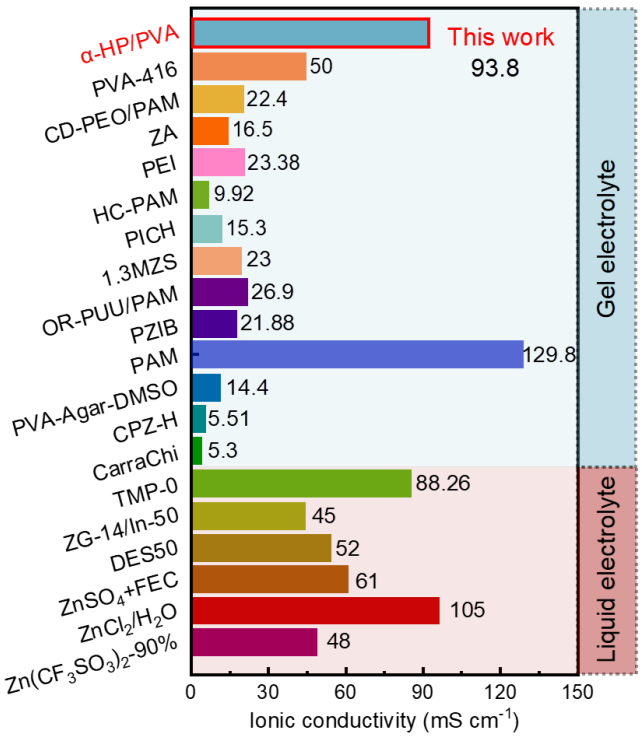

Figure S4. Comparison of ionic conductivity of electrolytes reported recently.[5-23]

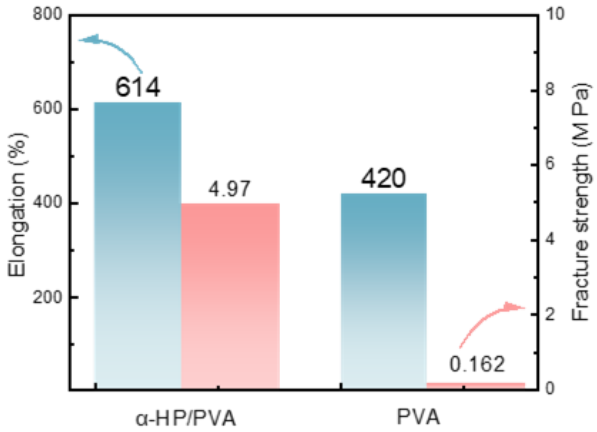

Figure S5. Comparison of elongation and fracture strength of α-HP/PVA and PVA hydrogel electrolytes.

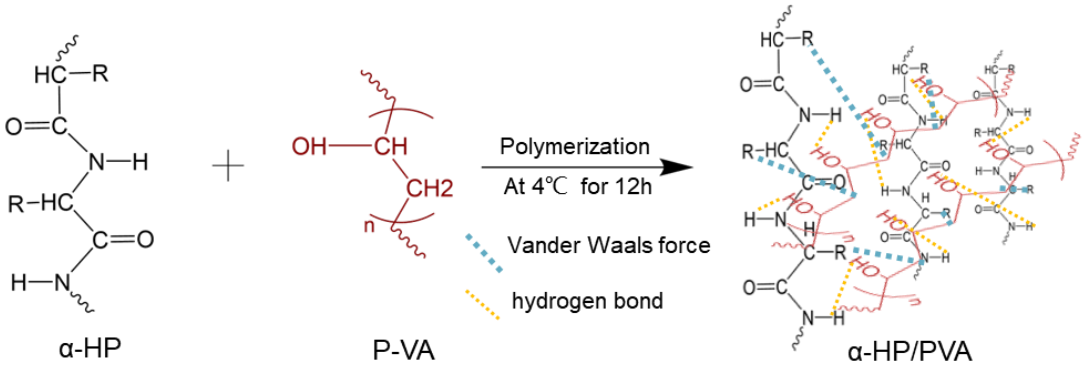

Figure S6. Network cross-linking of α-HP and P-VA.

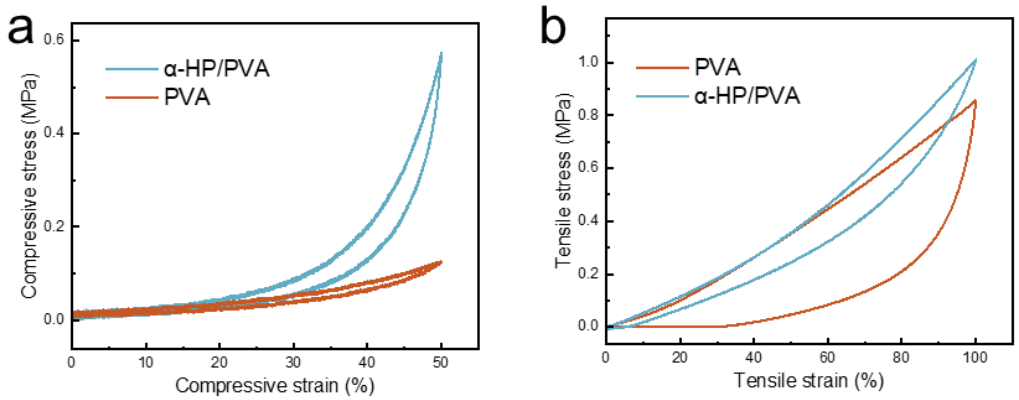

Figure S7. (a) Typical compression-relaxation cycles and (b) typical stretching-relaxation cycles of α-HP/PVA and PVA hydrogel electrolytes.

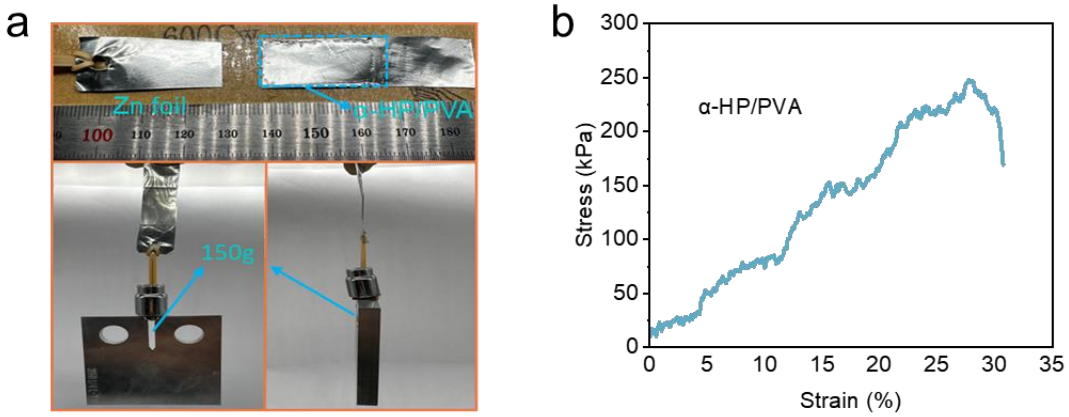

Figure S8. (a) The optical photographs show the adhesive performance of the α-HP/PVA hydrogel electrolyte. (b) Representative stress–strain curves of lap shear test on two pieces of Zn foils adhered by the α-HP/PVA hydrogel electrolyte.

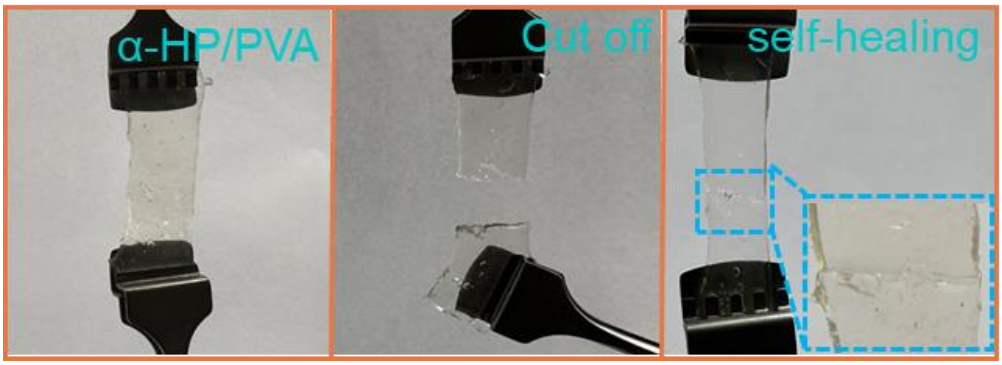

Figure S9. The α-HP/PVA hydrogel electrolyte could be self-healing by keeping at low temperature (2~5℃) for 2 h.

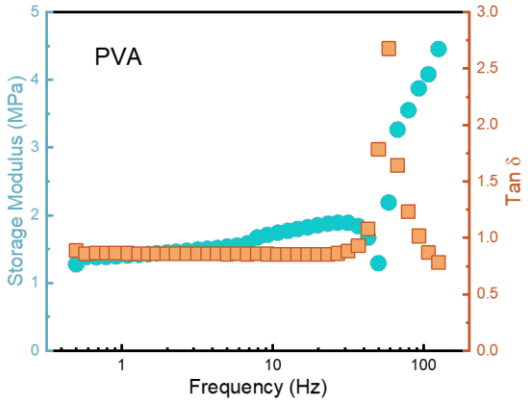

Figure S10. Dynamic mechanical analysis of PVA hydrogel electrolyte under a small strain.

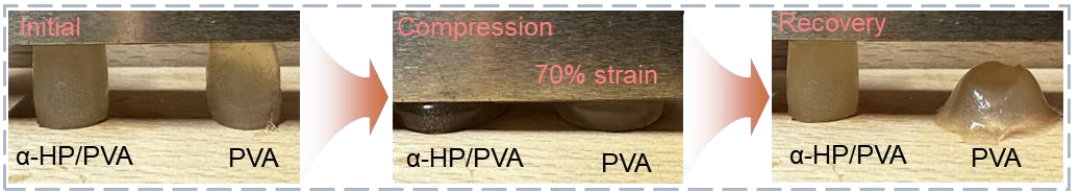

Figure S11. Comparison of compression property of PVA and α-HP/PVA electrolytes.

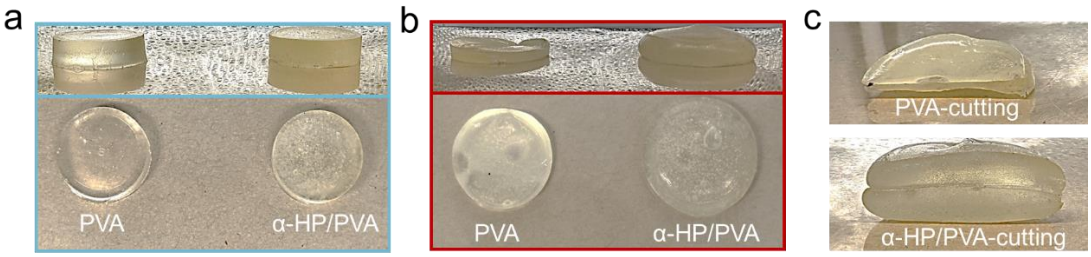

Figure S12. Photographs of different hydrogel electrolytes placed at room temperature (25 °C) and 30% humidity for different times. (a) 0 h, (b) 96 h, (c) Hydrogel electrolytes were cut after being placed for 96 h.

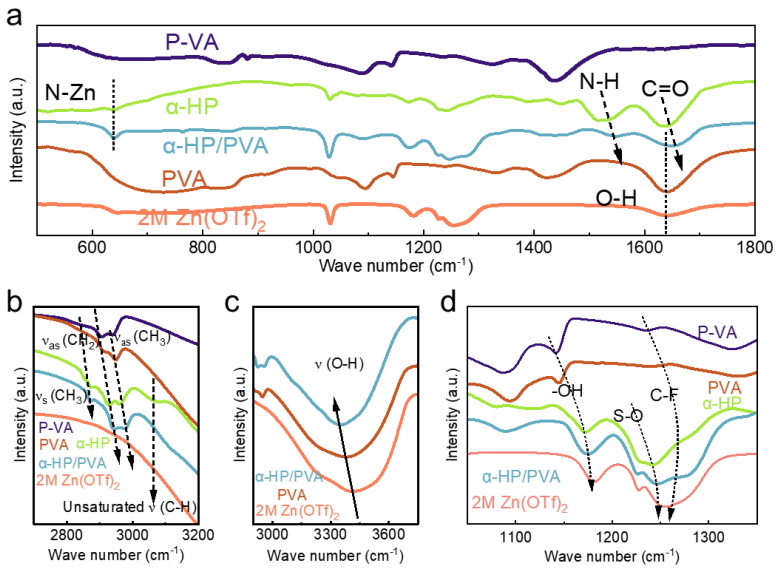

Figure S13. FT-IR spectra of P-VA, α-HP, 2M $Zn(OTf)_2$, PVA and α-HP/PVA in different wave number. (a) 500-1800 cm^{-1}. (b) 2800-3700 cm^{-1}. (c) 2700-3200 cm^{-1}. (d) 1050-1350 cm^{-1}.

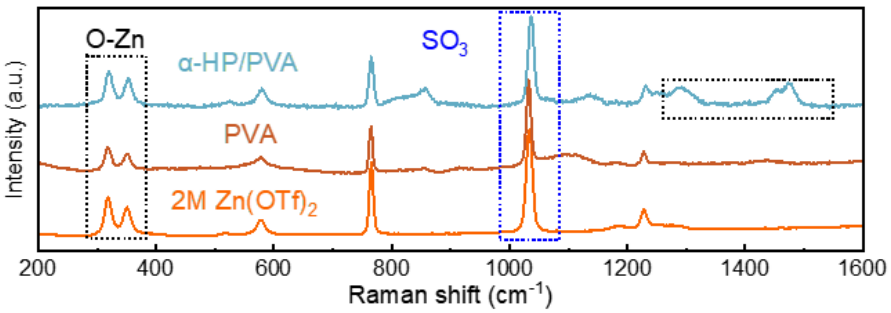

Figure S14. Raman spectra of 2M $Zn(OTf)_2$, PVA and α-HP/PVA in 200-1600 cm^{-1}.

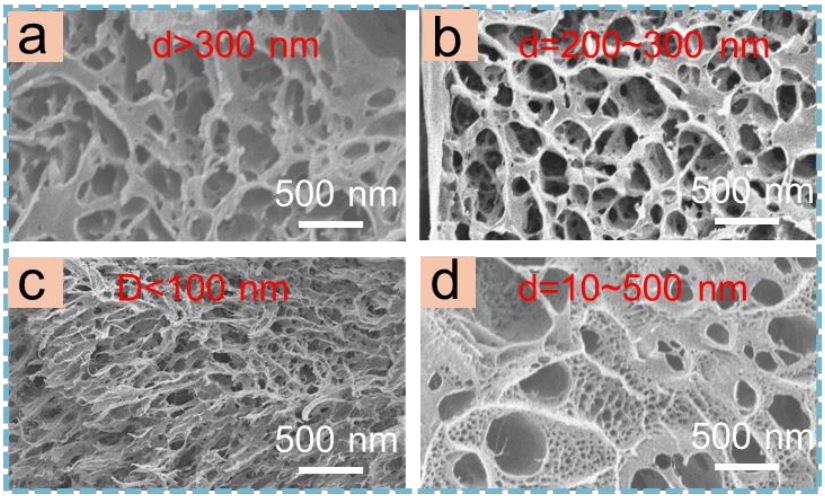

Figure S15. SEM images of hydrogel skeletons for different electrolytes. (a) PVA. (b) α-HP/$PVA_{0.5:1}$. (c) α-HP/$PVA_{1:1}$. (d) α-HP/$PVA_{2:1}$.

As shown in **Figure S15a**, the skeleton structure of PVA hydrogel electrolyte is unstable and with large pore size (over 300 nm). When α-HP and P-VA are added with a mass ratio of 0.5:1 (**Figure S15b**), a hydrogel skeleton with a stable structure and uniform pore size (d=200~300 nm) could be formed, indicating that α-HP is beneficial for stabilizing the hydrogel skeleton. When the content of α-HP is continued to increase (α-HP: P-VA=1:1) (**Figure S15c**), the skeleton pore size is further reduced (d<100 nm) and the hydrogel electrolyte (α-HP/PVA) exhibits the optimal elasticity properties and the highest water retention rate. However, when the mass ratio is increased to 2:1 (**Figure S15d**), the pore size range of the hydrogel skeleton becomes wider (10-500 nm), suggesting that too much α-HP could make the pore size inhomogeneous unfavorable for the rapid conduction of Zn^{2+}.

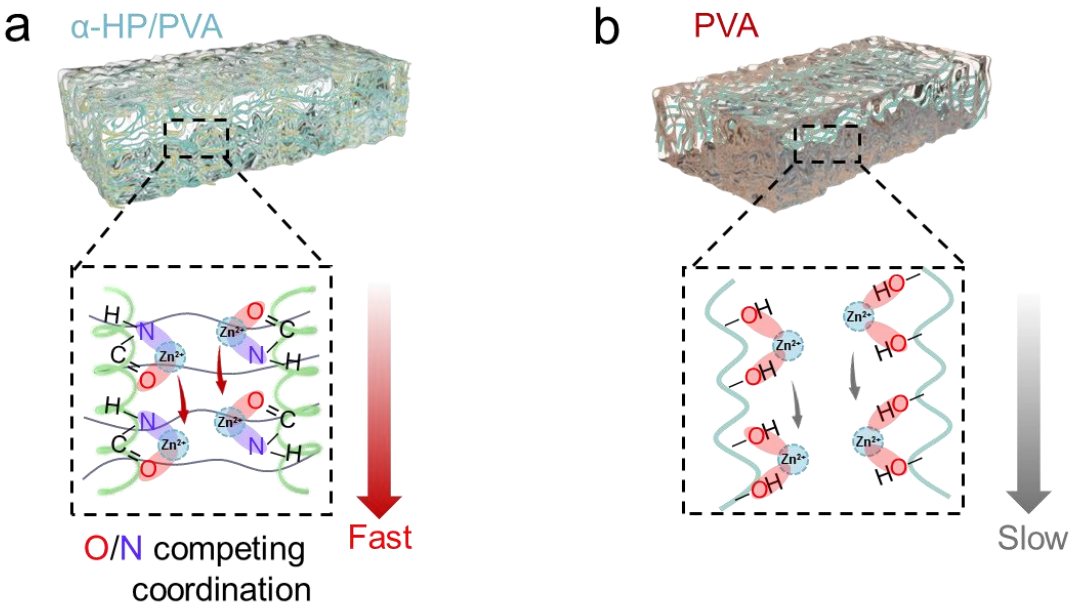

Figure S16. Transport mechanism of Zn^{2+} in (a) α-HP/PVA and (b) PVA.

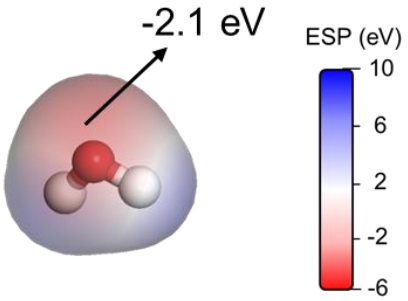

Figure S17. Electrostatic potential mapping of H_2O.

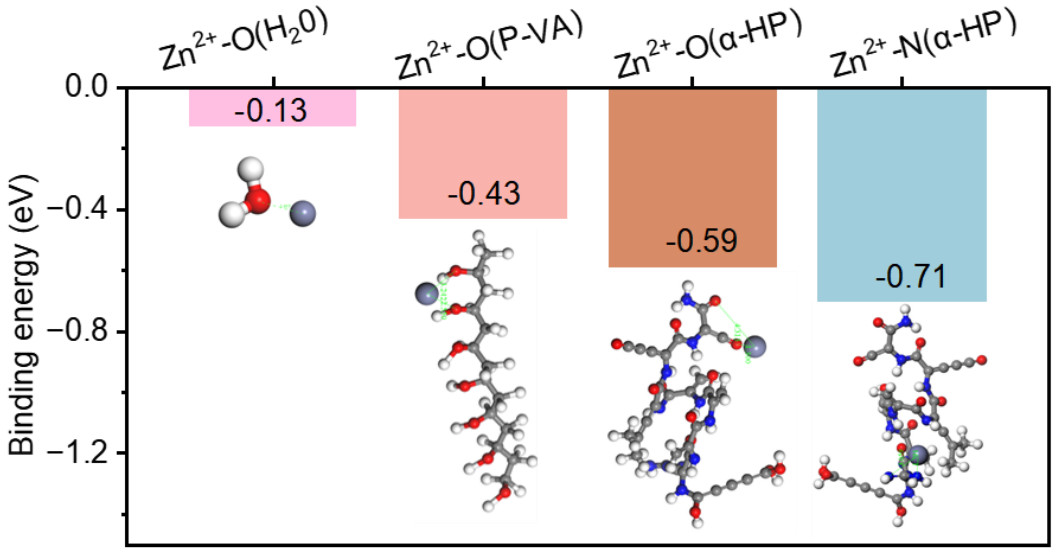

Figure S18. Comparison of the binding energies of Zn^{2+}-O(H_2O), Zn^{2+}-O(PVA), Zn^{2+}-O(α-HP) and Zn^{2+}-N(α-HP).

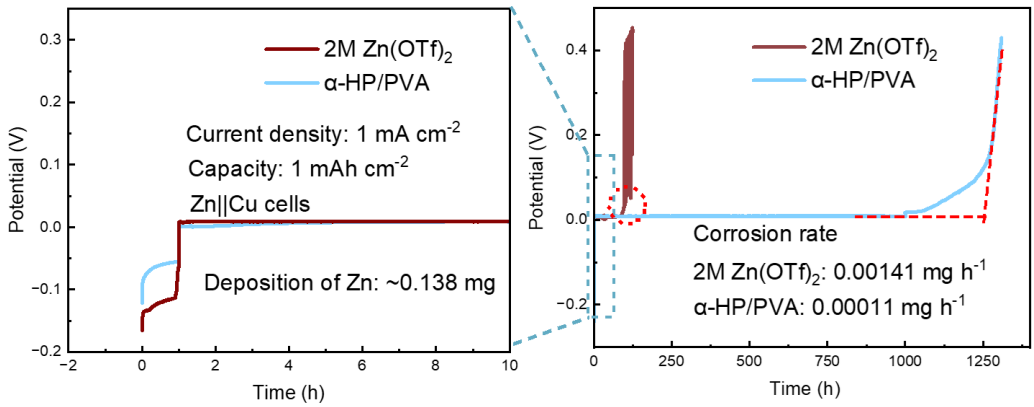

Figure S19. Quantitative corrosion testing of Zn anodes in α-HP/PVA and 2 M $Zn(OTf)_2$ electrolytes.

Note: To compare the corrosion resistance quantitatively, we assembled Zn||Cu cells with different electrolytes and deposited 1 mAh cm^{-2} of Zn metal, and then performed potentiostatic monitoring. After deposition, the initial monitoring voltage of the cell is ~0 V. As the zinc on the surface of the Cu electrode is continuously corroded, the monitoring voltage will change. When the voltage increases sharply, it can be determined that the zinc on the Cu electrode surface is completely corroded, and the corresponding time is used to calculate the corrosion rate.

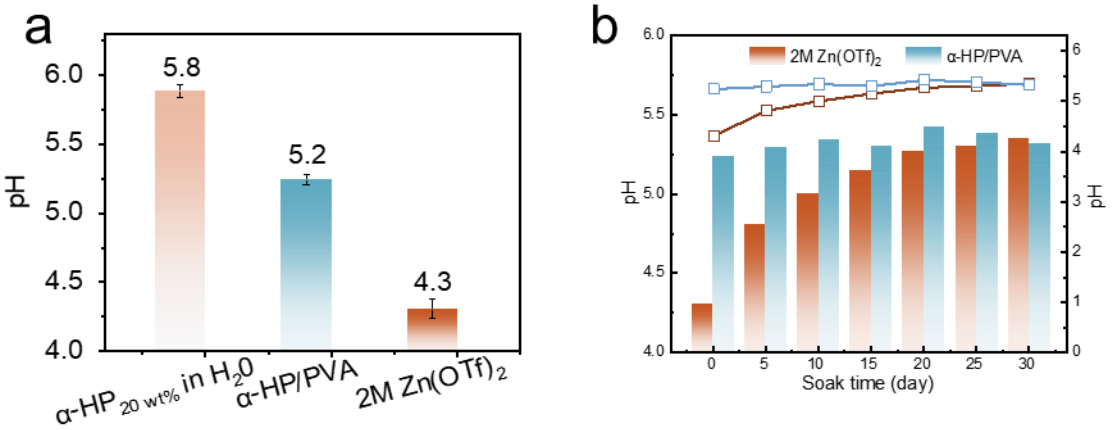

Figure S20. (a) Comparison of pH for different electrolytes. (b) The variation of pH of the electrolyte after Zn anode soaking for different time.

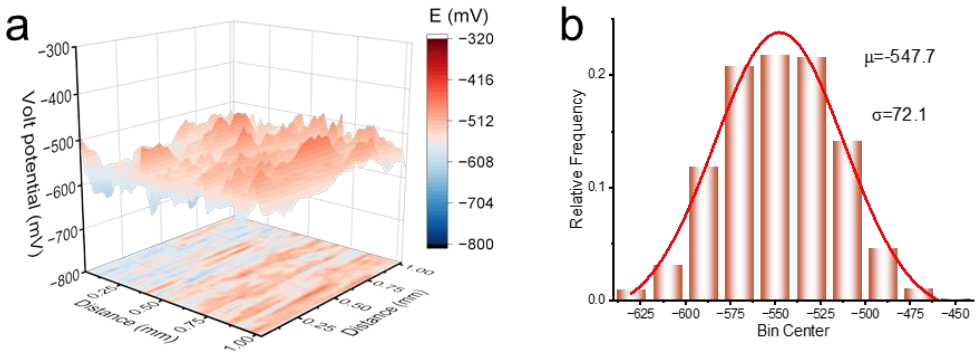

Figure S21. (a) Volta potential maps via scanning Kelvin probe (SKP) testing bare Zn anode, and (b) the corresponding data statistics of Volta potential by Gaussian fitting.

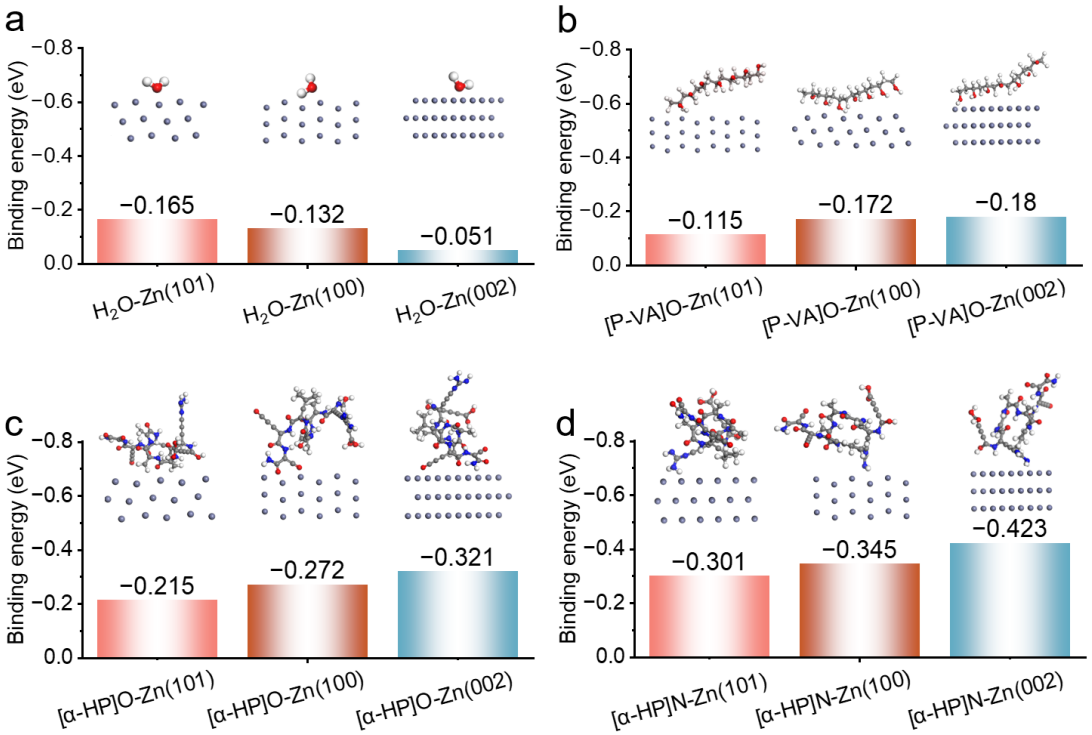

Figure S22. Absorption energies of H_2O, P-VA, and α-HP on different Zn crystal planes. (a) O in H_2O. (b) O in P-VA. (c) O in α-HP. (d) N in α-HP.

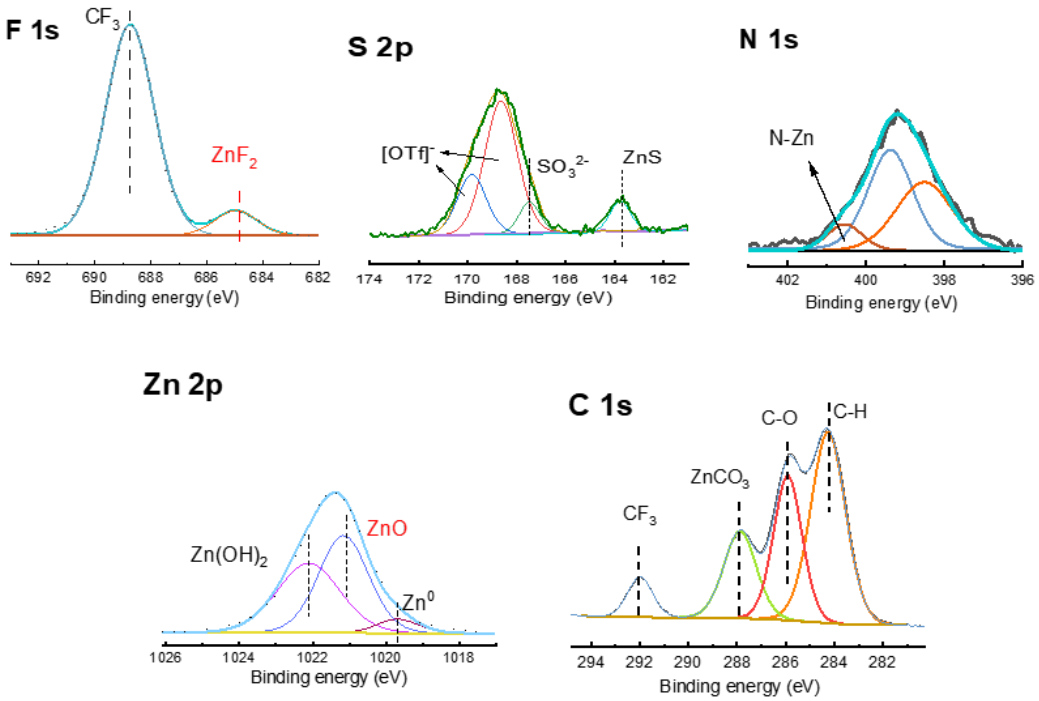

Figure S23. The related high-resolution XPS spectra comparison of F 1s, S 2p, N 1s, Zn 2p and C 1s in Zn anode after cycling in α-HP/PVA electrolyte.

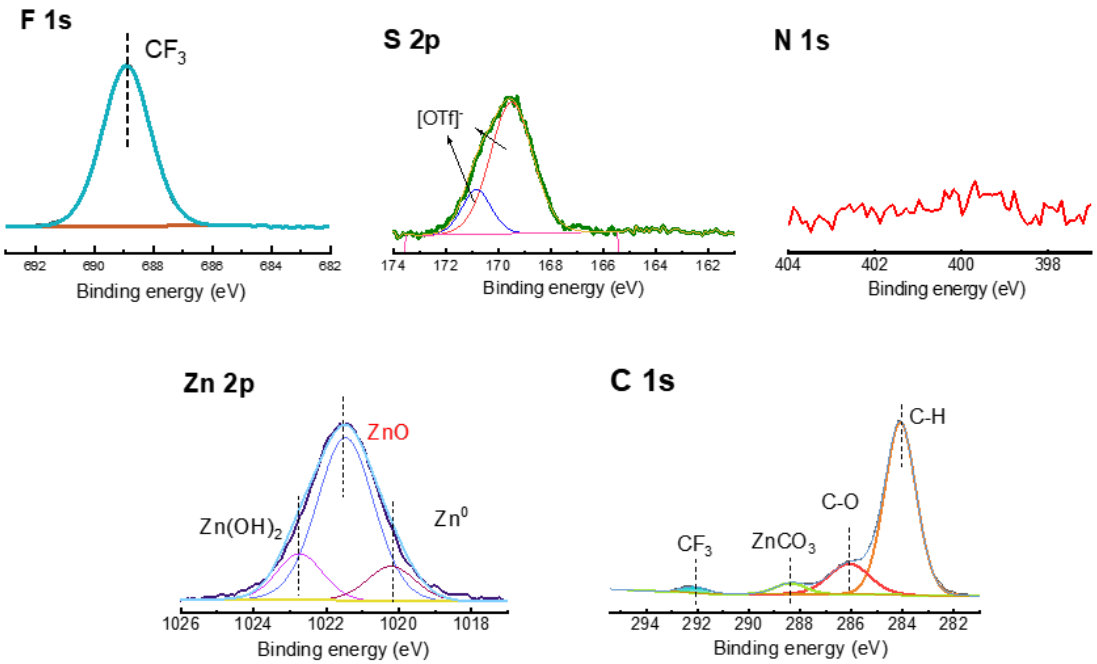

Figure S24. The related high-resolution XPS spectra comparison of F 1s, S 2p, N 1s, Zn 2p and C 1s in Zn anode after cycling in 2 M $Zn(OTf)_2$ electrolyte.

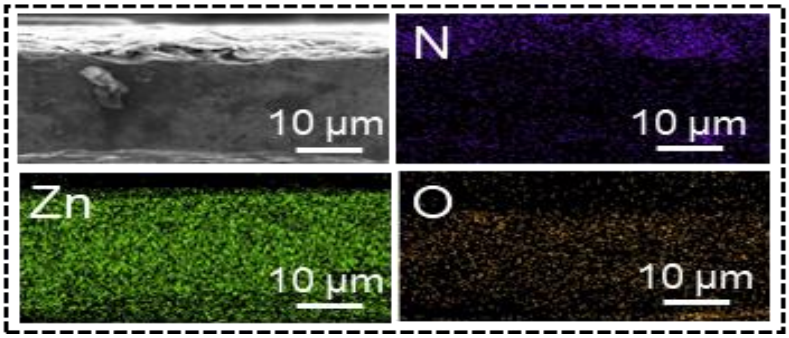

Figure S25. The EDS mapping of Zn anode cross section after cycling in α-HP/PVA electrolyte.

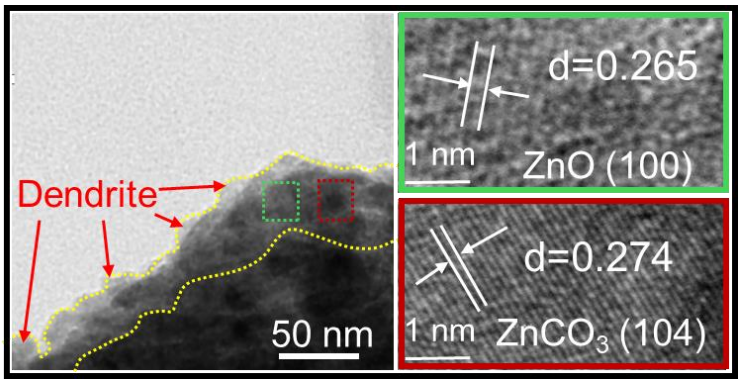

Figure S26. The TEM image and HRTEM magnified images of the anode cycled in 2M $Zn(OTf)_2$.

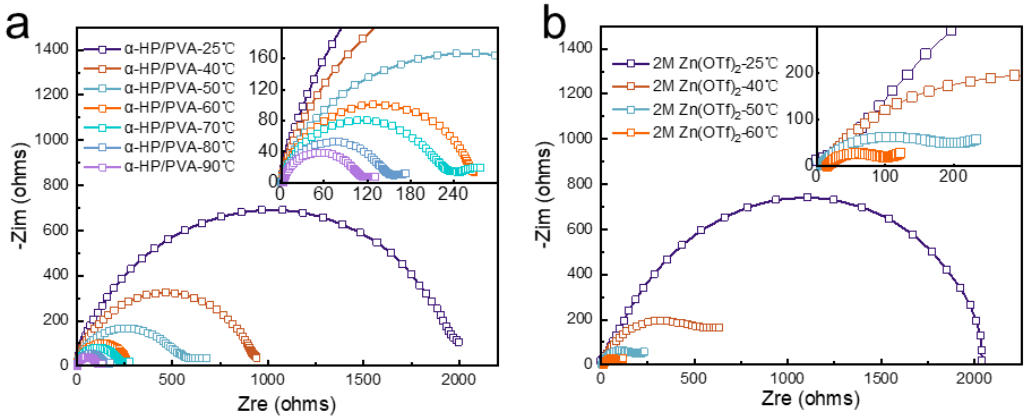

Figure S27. EIS of Zn|α-HP/PVA|Zn (a) and Zn|2M $Zn(OTf)_2$|Zn (b) symmetric cells at different temperatures.

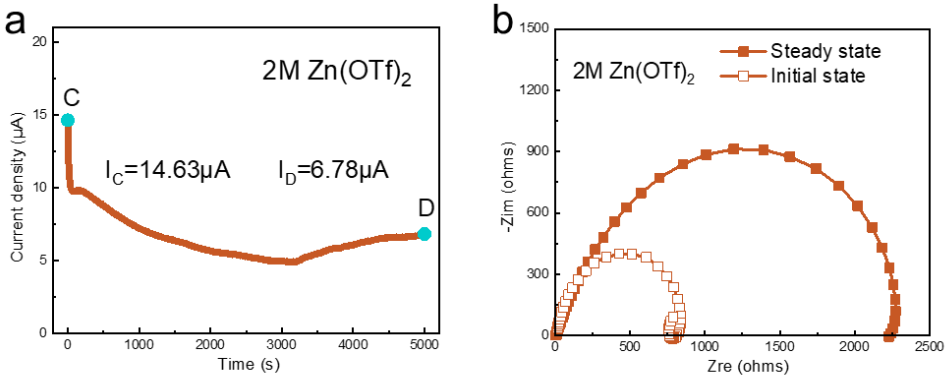

Figure S28. (a) Current variations of the Zn|2M $Zn(OTf)_2$|Zn symmetric cell at room temperature with potentiostatic polarization (ΔV=10 mV). (b) Nyquist plots of Zn|2M $Zn(OTf)_2$|Zn at the before potentiostatic polarization (initial state, C) and after 3600 s of potentiostatic polarization (steady state, D).

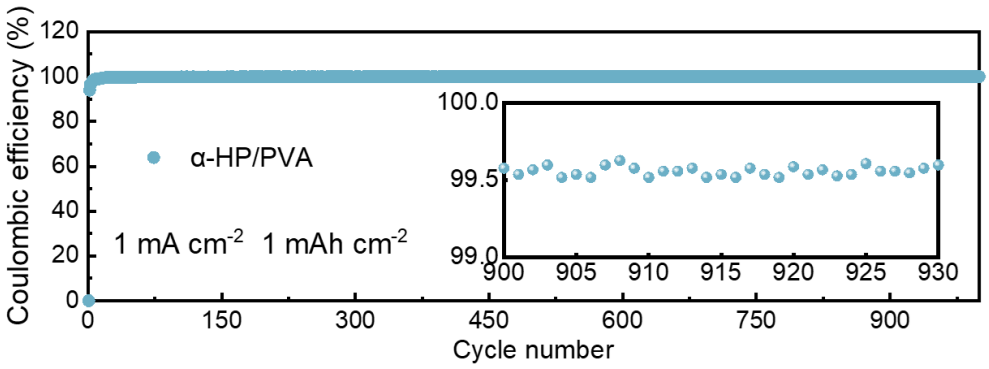

Figure S29. Coulombic efficiency of Zn|α-HP/PVA|Cu half cell after 990 cycles at 1 mA cm^{-2}.

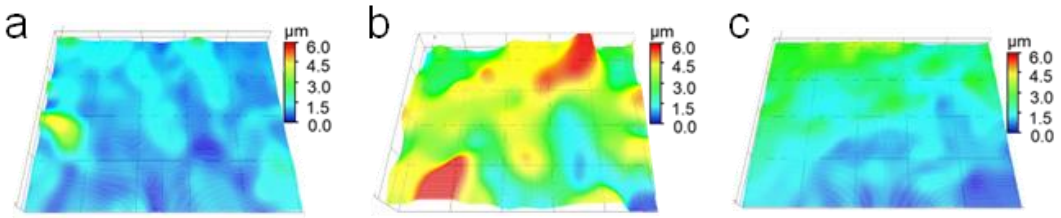

Figure S30. Three-dimensional microscope was used to characterize the surface morphology of Zn anodes. (a) Initial state. the Zn anodes after a long-term galvanostatic cycling in 2M $Zn(OTf)_2$ (b) and α-HP/PVA (c) electrolytes (0.1 mA cm^{-2}/1 mAh cm^{-2}).

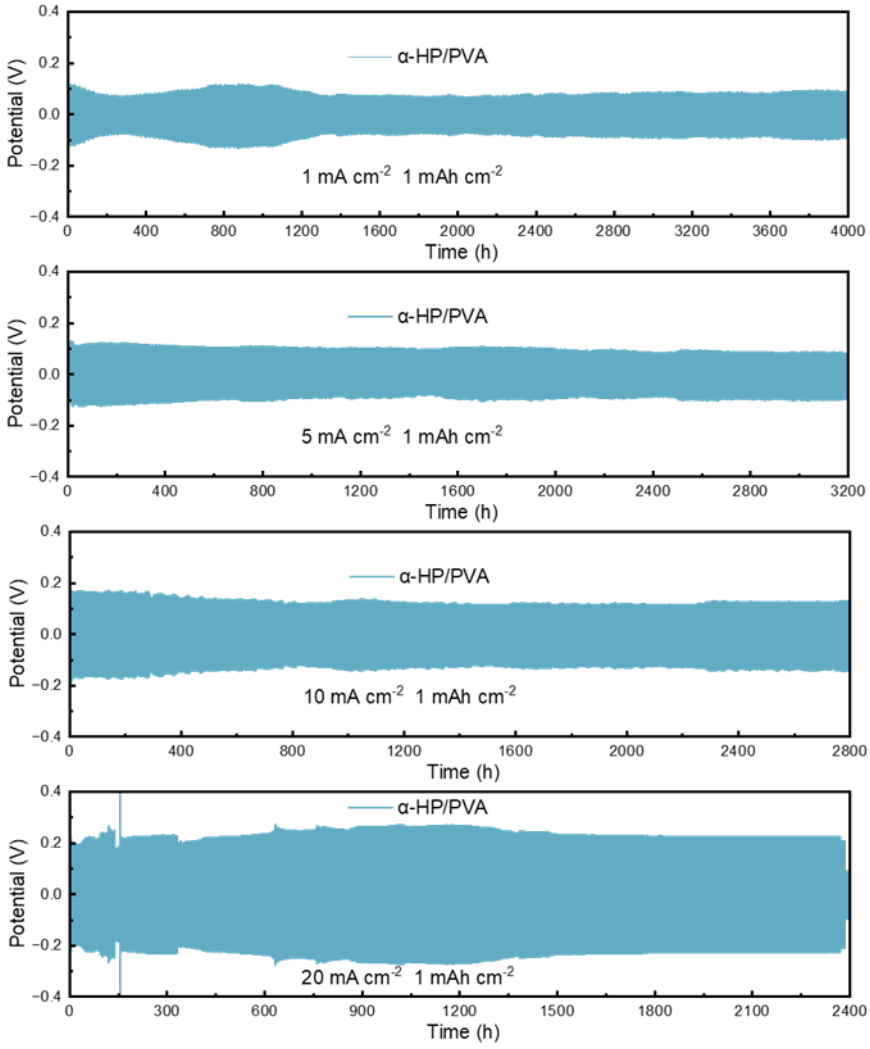

Figure S31. Long-term galvanostatic cycling of symmetric cells with α-HP/PVA electrolyte at different current density.

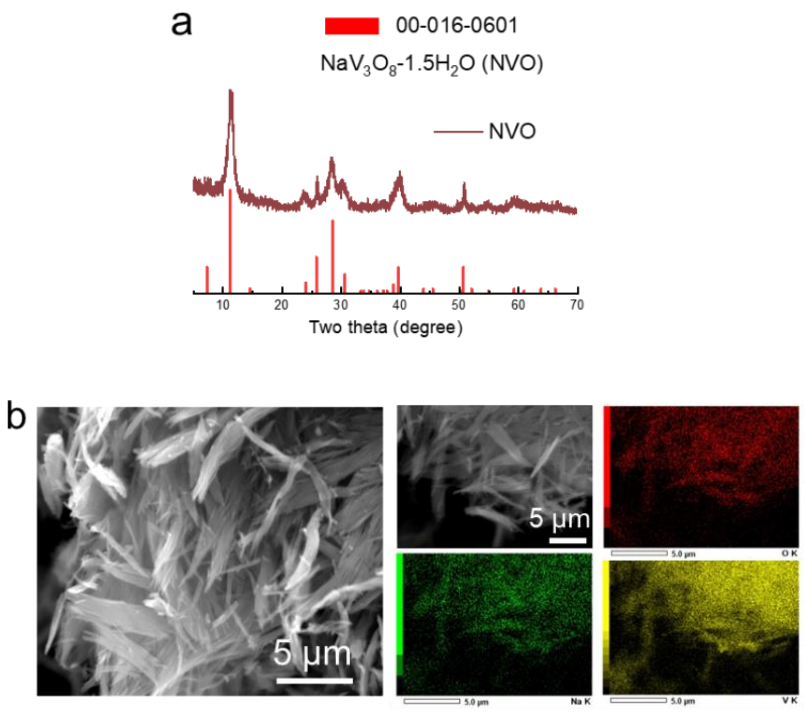

Figure S32. The XRD patterns (a) and SEM image (b) of NVO.

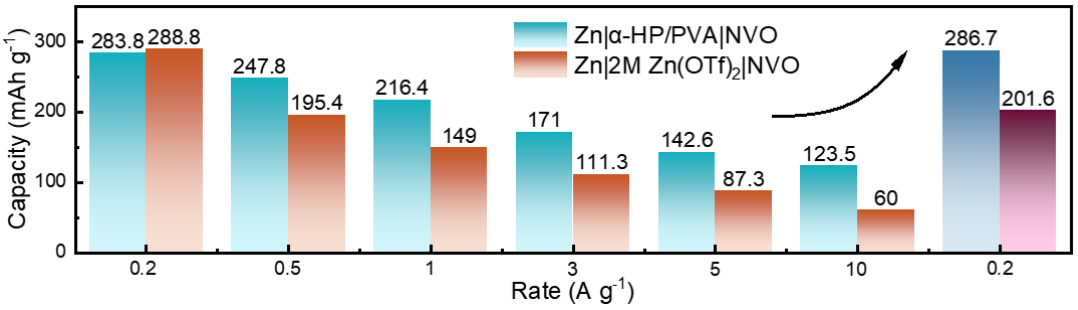

Figure S33. Capacity-Rate histogram of Zn|α-HP/PVA|NVO and Zn|2M $Zn(OTf)_2$|NVO full cells.

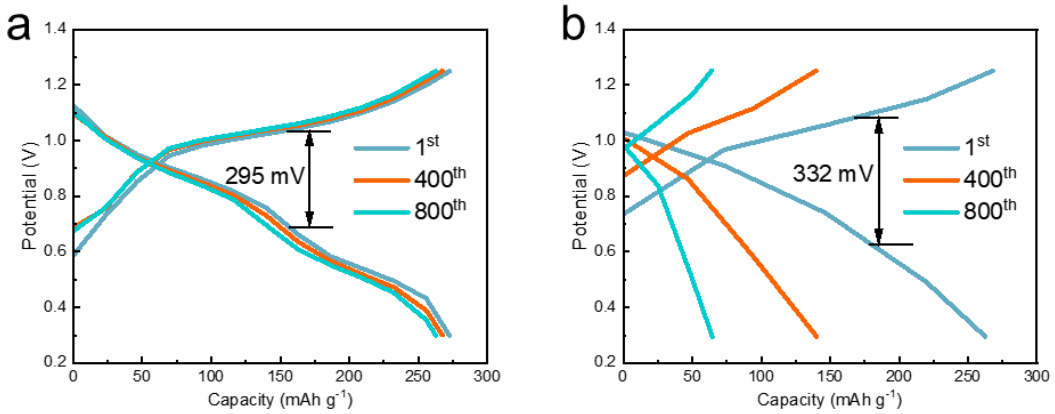

Figure S34. The charge and discharge curves of Zn|α-HP/PVA|NVO (a) and Zn|2M $Zn(OTf)_2$|NVO (b) full cells at 1 A g^{-1}.

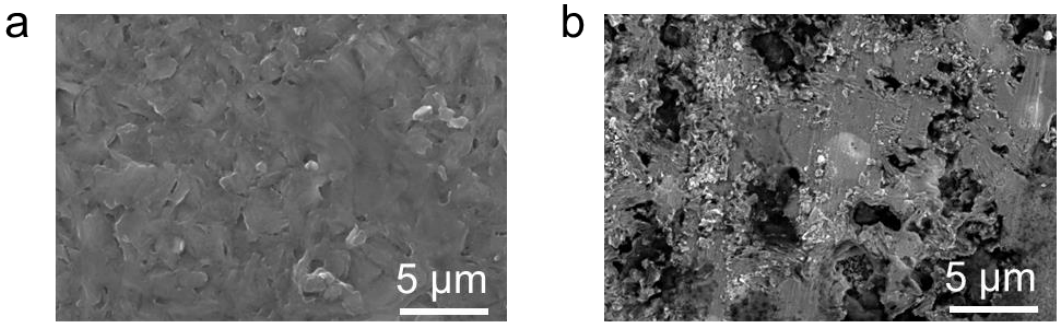

Figure S35. Surface SEM images of Zn anode after cycling test of Zn|α-HP/PVA|NVO (a) and Zn|2M $Zn(OTf)_2$|NVO (b) full cells at 1 A g^{-1}.

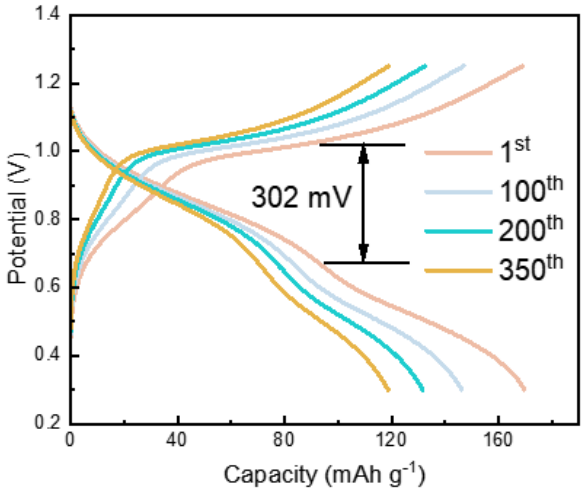

Figure S36. The charge and discharge curves of Zn|α-HP/PVA|NVO pouch cell at 1 A g^{-1}.

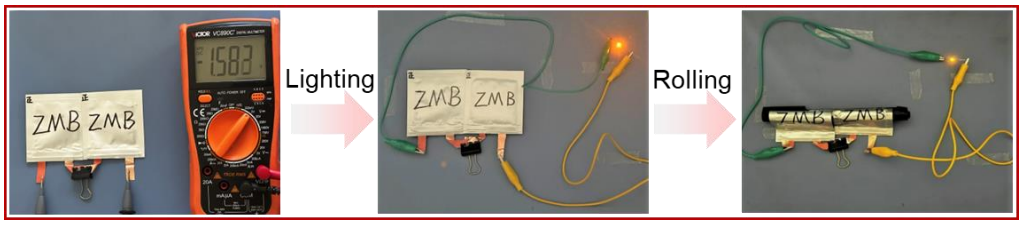

Figure S37. Photographs of the voltage display and powering the yellow LED at different bending angles for two pouch cells.

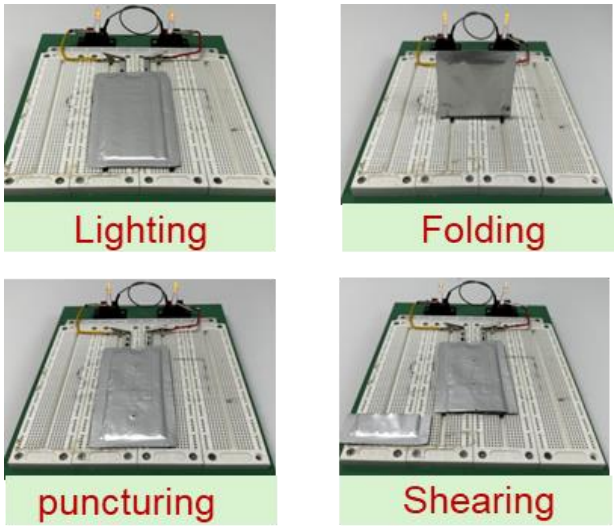

Figure S38. Other view photographs of the Zn|α-HP/PVA|NVO pouch cell powering the yellow LED in different states.

Table 1. The original data of ionic conductivity in figure 1b.

electrolyte	L (cm)	R (Ω)	σ (mS/cm)
PVA	0.1738	5.81	38.1
α-HP/$PVA_{0.5:1}$	0.1047	2.11	63.2
α-HP/$PVA_{1:1}$	0.0832	1.13	93.8
α-HP/$PVA_{2:1}$	0.1283	3.91	41.8

Note: The thickness of α-HP/$PVA_{x:1}$ hydrogel electrolyte is 0.1±0.02 cm, and the thickness of PVA hydrogel electrolyte is thicker (0.1738 cm) because of the poor mechanical property.

Ionic conductivities (σ) are calculated according to the following equation:

$$\sigma = L/RS$$

where R represents the resistance according to EIS measurement, L represents the thickness of hydrogel electrolyte, and S is the area (0.785 cm^2).

Table 2. Composition of different hydrogel electrolytes.

	H_2O(g) (wt.%)	**PVA(g) (wt.%)**	**α-HP(g) (wt.%)**	**$Zn(OTf)_2$(g) (wt.%)**	**glycerol(g) (wt.%)**	**Ionic conductivity (mS/cm)**
1	10 g (68.4 wt.%)	0.88 g (6.0 wt.%)	0	3.63 g (1 M) (24.8 wt.%)	0.12 g (0.8 wt.%)	38.1
2	10 g (66.3 wt.%)	0.88 g (5.8 wt.%)	0.44 g (2.9 wt.%)	3.63 g (1 M) (24.1 wt.%)	0.12 g (0.9 wt.%)	63.2
3	***10 g (64.5 wt.%)***	***0.88 g (5.67 wt.%)***	***0.88 g (5.67 wt.%)***	***3.63 g (1 M) (23.4 wt.%)***	***0.12 g (0.76 wt.%)***	***93.8***
4	10 g (61 wt.%)	0.88 g (5.4 wt.%)	1.76 g (10.7 wt.%)	3.63 g (1 M) (22.1 wt.%)	0.12 g (0.8 wt.%)	41.8
5	10 g (78.2 wt.%)	0.88 g (6.9 wt.%)	0.88 g (6.9 wt.%)	0.91 g (0.25 M) (7.1 wt.%)	0.12 g (0.9 wt.%)	35.3
6	10 g (72.9 wt.%)	0.88 g (6.4 wt.%)	0.88 g (6.4 wt.%)	1.82 g (0.5 M) (13.3 wt.%)	0.12 g (1 wt.%)	52
7	10 g (52.2 wt.%)	0.88 g (4.6 wt.%)	0.88 g (4.6 wt.%)	7.26 g (2 M) (37.9 wt.%)	0.12 g (0.7 wt.%)	58.6

[1] L. Zhang, F. Hu, S. Zhu, Y. Lin, Z. Meng, R. Yu and X. Liu. *Small,* 2020, **16**, 2000128.

[2] X. Xu, S. Li, H. Yan, J. Du, S. Yang and B. Li. *Adv. Funct. Mater*., 2023, **34**, 2308661.

[3] H. Yan, C. Han, S. Li, J. Liu, J. Ren, S. Yang and B. Li, *Chem. Eng. J.,* 2022**, 442**, 136081.

[4] J. He, Y. Tang, G. Liu, H. Li, M. Ye, Y. Zhang, Q. Yang, X. Liu and C. Li, *Adv. Energy Mater*., 2022, **12**, 2202661.

[5] X. Wang, Y. Ying, S. Chen, Q. Meng, H. Huang and L. Ma, *Nano Energy*, 2024, **119**, 109099.

[6] Y. Yan, S. Duan, B. Liu, S. Wu, Y. Alsaid, B. Yao, S. Nandi, Y. Du, T. W. Wang, Y. Li and X. He, *Adv. Mater*., 2023, 2211673.

[7] F. Wang, J. Zhang, H. Lu, H. Zhu, Z. Chen, L. Wang, J. Yu, C. You, W. Li, J. Song, Z. Weng, C. Yang and Q. Yang, *Nat. Commun*., 2023, **14**, 4211.

[8] H. Lu, J. Hu, X. Wei, K. Zhang, X. Xiao, J. Zhao, Q. Hu, J. Yu, G. Zhou and B. Xu, *Nat. Commun*., 2023, **14**, 4435.

[9] M. Li, C. Xi, X. Wang, L. Li, Y. Xiao, Y. Chao, X. Zheng, Z. Liu, Y. Yu and C. Yang, *Small*, 2023, 2301569.

[10] M. Jiao, L. Dai, H. Ren, M. Zhang, X. Xiao, B. Wang, J. Yang, B. Liu, G. Zhou and H. Cheng, *Angew. Chem., Int. Ed*., 2023, **62**, e202301114.

[11] Y. Hao, D. Feng, L. Hou, T. Li, Y. Jiao and P. Wu, *Adv. Sci*., 2022, **9**, 2104832.

[12] K. Zhu, J. Luo, D. Zhang, N. Wang, S. Pan, S. Zhou, Z. Zhang, G. Guo, P. Yang, Y. Fan, S. Hou, Z. Shao, S. Liu, L. Lin, P. Xue, G. Hong, Y. Yang and Y. Yao, *Adv. Mater*., 2024, 2311082.

[13] Z. Yang, Q. Zhang, T. Wu, Q. K. J. M. Li, J. Gan, S. Xiang, H. Wang, C. Hu, Y. Tang and H. Wang, *Angew. Chem., Int. Ed*., 2024, **63**, e202317457.

[14] J. Yang, T. Xiao, T. Xiao, J. Li, Z. Yu, K. Liu, P. Yang and H. Fan, *Adv. Mater.,* 2024, **36**, 2313610.

[15] Z. Liu, Z. Chen, S. Lei, B. Lu, S. Liang, J. Li and J. Zhou, *Adv. Mater*., 2024, 2308836.

[16] Q. Liu, X. Ou, Y. Niu, L. Li, D. Xing, Y. Zhou and F. Yan, *Angew. Chem., Int.*

Ed., 2024, e202317944.

[17] C. Li, W. Wang, J. Luo, W. Zhuang, J. Zhou, S. Liu, L Lin, W. Gong, G. Hong, Z. Shao, J. Du, Q. Zhang and Y. Yao, *Adv. Mater*., 2024, 2313772.

[18] H. Xia, G. Xu, X. Cao, C. Miao, H. Zhang, P. Chen, Y. Zhou, W. Zhang and Z. Sun, *Adv. Mater*., 2023**, 35**, 2301996.

[19] S. Zhang, J. Hao, Y. Zhu, H. Li, Z. Lin and S. Qiao, *Angew. Chem., Int. Ed*., **2023**, e202301570.

[20] D. Xie, Y. Sang, D. Wang, W. Diao, F. Tao, C. Liu, J. Wang, H. Sun, J. Zhang and X. Wu, *Angew. Chem., Int. Ed*., 2023, **135**, e202216934.

[21] S. Wang, G. Liu, W. Wan, X. Li, J. Li and C. Wang, *Adv. Mater.,* 2024, **36**, 2306546.

[22] J. Wan, R. Wang, Z. Liu, S. Zhang, J. Hao, J. Mao, H. Li, D. Chao, L. Zhang and C. Zhang, *Adv. Mater*., 2023, 2310623.

[23] W. Wang, S. Chen, X. Liao, R. Huang, F. Wang, J. Chen, Y. Wang, F. Wang and H. Wang, Nat. Commun., 2023, **14**, 5443.